J|A|C|S ARTICLES

Published on Web 09/14/2010

Synthesis, Crystal Structure, and Properties of $Mg_xB_{50}C_8$ or $Mg_x(B_{12})_4(CBC)_2(C_2)_2$ ($x = 2.4-4$)

Volker Adasch,[†] Melanie Schroeder,[‡] Dominik Kotzott,[‡] Thilo Ludwig,[‡] Natascha Vojteer,[‡] and Harald Hillebrecht*[,‡,§]

DRONCO AG, Wiesenmühle 1, D-95632 Wunsiedel, Germany, Institut für Anorganische und Analytische Chemie, Albert-Ludwigs-Universität Freiburg, Albertstrasse 21, D-79104 Freiburg, Germany, and Freiburger Materialforschungszentrum FMF, Stefan-Maier-Strasse 25, D-79104 Freiburg, Germany

Received April 13, 2010; E-mail: harald.hillebrecht@ac.uni-freiburg.de

Abstract: Single crystals of a new magnesium boride carbide $Mg_xB_{50}C_8$ ($x = 2.4-4$) were synthesized from the elements in a metallic melt using tantalum ampules. Crystals were characterized by single crystal X-ray diffraction and electron microprobe analysis. The variation of the Mg content results from different reaction conditions. The composition $Mg_{\sim 3}B_{50}C_8$ is by far the most favored. It fulfills the electron counting rules of Wade and Longuet-Higgins and thus explains the light-green to yellow transparent color. The structure of $Mg_{\sim 3}B_{50}C_8$ ($C2/m$, $Z = 1$, $a = 8.9384(12)$ Å, $b = 5.6514(9)$ Å, $c = 9.6021(13)$ Å, $\beta = 105.86(1)°$) consists of B_{12} icosahedra. The icosahedra are interconnected by four exohedral B−B bonds to layers. The layers are connected to a three-dimensional covalent network by C_2 and CBC units and further exohedral B−B bonds. The Mg sites are partially occupied. Different site occupation factors cause the various compositions and colors ($Mg_{2.4}B_{50}C_8$, brown; $Mg_4B_{50}C_8$, black). The vibrational spectra show the modes of B_{12} icosahedra and C_2 and CBC units as well. Measurements of the microhardness according to Vickers and Knoop revealed remarkably high values of $H_V = 3286$ (32.0 GPa) and $H_K = 3165$ (31.5 GPa), which exceed the values of B_4C. Optical spectra reveal a band gap of 2.7 eV for $Mg_{\sim 3}B_{50}C_8$, in agreement to the observed color. This justifies an ionic description, and the formula can be written as $(Mg^{2+})_3(B_{12}^{2-})_4(CBC^+)_2(C_2)_2$.

Introduction

Because boron-rich borides and boride carbides contain a great variety of boron polyhedra, they form their own class of compounds and show an unique structure chemistry[1] and physical properties.[2,3] Furthermore, they are of growing interest to a number of applications in material sciences, for example, as high temperature materials,[3] abrasives,[4] composites,[5] high T_c superconductors,[6] high temperature semiconductors,[7] and high temperature thermoelectrics.[8] Our previous investigations have shown that the use of molten metals gives a synthetic access to new borides and boride carbides not obtained by conventional high temperature methods.[9−12] Motivated by the discovery of superconductivity in MgB_2[13] and the excellent material properties of Mg alloys,[14] we extended this method to compounds containing Li[15,16] and Mg[17−21] by use of h-BN crucibles and tantalum ampules.

[†] DRONCO AG.
[‡] Albert-Ludwigs-Universität Freiburg.
[§] Freiburger Materialforschungszentrum FMF.

(1) (a) Matkovich, V. I. *Boron and Refractory Borides*; Springer-Verlag: Berlin, 1977. (b) Lundström, T. In *Encyclopedia of Inorganic Chemistry*; King, R. B., Ed.; Wiley: New York, 1994. (c) Albert, B.; Hillebrecht, H. *Angew. Chem.* **2009**, *121*, 8794–8824; *Angew. Chem., Int. Ed.* **2009**, *48*, 8640–8668.
(2) (a) Werheit, H. *Boron in Landolt-Börnstein*; Springer-Verlag: Berlin, 1998; Vol. 41C. (b) He, J.; Wu, E.; Wang, H.; Liu, R.; Tian, Y. *Phys. Rev. Lett.* **2005**, *94*, 015504. (c) Cao, L.; Zhang, Z; Sun, L.; Gao, C. *Adv. Mater.* **2001**, *13*, 1701–1704.
(3) (a) Chawla, K. K. *Ceramic Composites*; Chapman & Hall: London, 1993. (b) Chou, T. W. *Structure and Properties of Composites in Material Science and Technology*; Verlag Chemie: Weinheim, Germany, 1993; Vol. 13. (c) Riedel, R., Ed. *Handbook of Ceramic Hard Materials*; Wiley-VCH: Weinheim, Germany, 2000.
(4) (a) Riedel, R. *Adv. Mater.* **1994**, *4*, 549–560. (b) Telle, R. *Chem. Unserer Zeit* **1988**, *22*, 93–99.
(5) (a) Halverson, D. C.; Pyzik, A.; Aksay, I. *Ceram. Eng. Sci. Proc.* **1985**, *6*, 736–744. (b) Pyzik, A.; Beamon, D. *J. Am. Ceram. Soc.* **1995**, *78*, 305–312.
(6) (a) Gunji, S.; Kamimura, H. *Phys. Rev. B* **1996**, *54*, 13665–13673. (b) Calandra, M.; Vast, N.; Mauri, F. *Phys. Rev. B* **2004**, *69*, 224505. (c) Matsuda, H.; Nakayama, T.; Kimura, K.; Murakami, Y.; Suematsu, H.; Kobayashi, M.; Higashi, I. *Phys. Rev. B* **1995**, *52*, 6102–6110.
(7) (a) Emin, D. *J. Solid State Chem.* **2004**, *177*, 1619–1623. (b) Samara, G. A.; Tardy, H. L.; Venturini, E.; Aselage, T. L.; Emin, D. *Phys. Rev. B* **1993**, *48*, 1468. (c) Emin, D. *Phys. Today* **1987**, *20*, 55. (d) Mori, T. In *Handbook on the Physics and Chemistry of Rare Earths*; Gschneidner, K. A., Bunzli, J. C., Pecharsky, V., Eds.; Elsevier: Amsterdam, 2008; Vol. 38, pp 106−173.
(8) Wood, C. *Rep. Prog. Phys.* **1988**, *51*, 459.
(9) (a) Hillebrecht, H.; Meyer, F. *Angew. Chem.* **1996**, *108*, 2655; *Angew. Chem., Int. Ed.* **1996**, *35*, 2499. (b) Hillebrecht, H.; Ade, M. *Angew. Chem.* **1998**, *110*, 981; *Angew. Chem., Int. Ed.* **1998**, *37*, 935. (c) Hillebrecht, H.; Gebhardt, K. *Angew. Chem.* **2001**, *113*, 1492; *Angew. Chem., Int. Ed.* **2001**, *40*, 1445.
(10) Adasch, V. Ph.D. Thesis, University Bayreuth, Germany, 2005.
(11) Vojteer, N. Ph.D. Thesis, University Freiburg, Germany, 2008.
(12) Schroeder, M. Ph.D. Thesis, University Freiburg, Germany, 2009.
(13) Nagamatsu, J.; Nakagawa, N.; Muranaka, T.; Zenitani, Y.; Akimitsu, J. *Nature* **2001**, *40*, 63–64.
(14) Kainer, K. U., Ed. *Magnesium Alloys and Their Applications*; Wiley-VCH, Weinheim, Germany, 2000.
(15) Vojteer, N.; Hillebrecht, H. *Angew. Chem.* **2006**, *118*, 172–175; *Angew. Chem., Int. Ed.* **2006**, *45*, 165–168.

When we started our investigations, MgB_2C_2[22] was the only ternary compound reported for the system Mg/B/C.[23] The crystal structure of MgB_2C_2 can be described as a heterographite where boron and carbon form hexagonal layers and magnesium is intercalated between the layers.

Recently we reported on the first boron rich boride carbides of magnesium: $Mg_2B_{24}C$,[20] *o*-$MgB_{12}C_2$, and *m*-$MgB_{12}C_2$.[21] In this contribution we report on $Mg_xB_{50}C_8$ ($x = 2.4-4$). The crystal structure combines the structural features of $Li_2B_{12}C_2$ and $LiB_{13}C_2$.[15] Besides the well-known B_{12} icosahedra, the crystal structure contains C_2 and linear CBC units. Therefore, the formula can be written as $Mg_x(B_{12})_4(CBC)_2(C_2)_2$. The Mg content varies between $x = 2.4$ and $x = 4.0$, depending on the conditions of the synthesis. For $Mg_3B_{50}C_8$ the composition was confirmed by EDX and WDX measurements on single crystals. The microhardness is remarkably high. Hardness measurements according to the methods of Vickers ($H_V = 32.0$ GPa) and Knoop ($H_K = 31.5$ GPa) reveal values that are even higher than those of B_4C, so $Mg_3B_{50}C_8$ is after diamond and *c*-BN is one of the hardest materials known. A new concept for superhard materials can be developed.

Experimental Section

1. Synthesis. 1.1. $Mg_{\sim 3}B_{50}C_8$. Single crystals of $Mg_{\sim 3}B_{50}C_8$ were synthesized from the elements in a Cu/Mg melt. Cu (powder, >250 mesh, p.A., Merck), Mg (powder, 325 mesh, 99.8%, Riedel-de Haen), B (crystalline, ~325 mesh, 99.7%, Alfa Aesar), and C (graphite powder, <100 μm, 99.9%, Heraeus) were mixed in a molar ratio of 12:4:3:0.1 and pressed into a pellet (~3 g). The pellet was put into a h-BN crucible and the crucible into a tantalum ampule, which was sealed by welding with an electric arc. The ampule was heated under an argon atmosphere up to 1573 K, held for 6 h, and cooled with 10 K/h to 873 K and with 100 K/h to room temperature. The ampule was opened, and the excess melt was dissolved in concentrated nitric acid. Single crystals of $Mg_{\sim 3}B_{50}C_8$ were transparent platelets of light-green to yellow or light-brown color with a size of up to 1 mm (Figure 1). As byproducts, single crystals of dark red MgB_7[10,11,24] and black MgB_{12}[18] were found.

Small amounts of $Mg_{\sim 3}B_{50}C_8$ were frequently observed as unexpected byproduct from syntheses of other borides[17,18] because commercial samples of boron can contain significant amounts of carbon. Furthermore $Mg_{\sim 3}B_{50}C_8$ can be formed together with other boride carbides[20,21] of Mg according to the equilibrium conditions during the crystal growth.

1.2. $Mg_{\sim 4}B_{50}C_8$. Black crystals of $Mg_4B_{50}C_8$ were found as a byproduct from a batch that yielded mostly MgB_7 and *o*-$MgB_{12}C_2$. In comparison to the previous synthesis the melt contained more Mg. The elements were mixed with a ratio Cu/Mg/B/C of 200:200:75:3. The ampule was heated under an argon atmosphere with 100 K/h to 1573 K, held for 25 h, and cooled with 10 K/h to 773 K and with 100 K/h to room temperature.

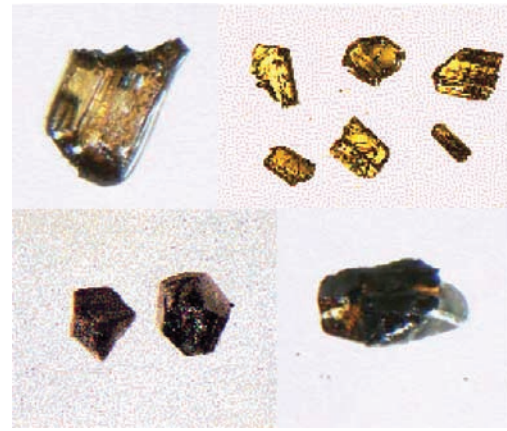

Figure 1. Upper row: Single crystals of $Mg_3B_{50}C_8$. Lower row: $Mg_{\sim 4}B_{50}C_8$, crystal size between 0.2 and 0.5 mm.

1.3. $Mg_{\sim 2.4}B_{50}C_8$. Brown crystals of $Mg_{2.4}B_{50}C_8$ (Figure 1) were found as a byproduct from a batch that yielded mostly MgB_9N.[23b] A Mg/Cu melt was used with a ratio Mg/Cu/B/C of 300:100:75:3. The ampule was heated under an argon atmosphere up to 1673 K, held for 30 h, and cooled with 60 K/h to room temperature. The formation of the nitride results from the reaction of the crucible, maybe caused by the higher temperature.

2. Structure Solution and Refinement. 2.1. $Mg_3B_{50}C_8$. Single crystal investigations of $Mg_3B_{50}C_8$ were done with a diffractometer equipped with Mo Kα radiation and an image plate detector (IPDS II, Fa. Stoe). A *C*-centered monoclinic unit cell was obtained with $a = 8.9384(12)$ Å, $b = 5.6514(9)$ Å, $c = 9.6021(13)$ Å, and $\beta = 105.86(1)°$. The measurement of 4180 intensities gave a data set of 1103 independent reflections (964 with $I > 2\sigma(I)$). Because of the low absorption coefficient (0.20 mm^{-1}), no correction of absorption effects was done. The additional reflection condition *hkl* with $h + k = 2n$ led to space group *C*2/*m* and the noncentrosymmetric space groups *C*2 and *Cm*, respectively. The structure solution by direct methods (SHELXL[25]) was started in *C*2/*m* and revealed a structure model with 11 independent nonmetal atoms and two Mg sites. The labeling of the atoms was done according to electron densities and bonding distances. B and C atoms were refined with anisotropic displacement parameters. Because partial and mixed occupations are well-known for boron rich borides, all occupation factors were refined separately as a free variable, but no significant deviations from full occupation were observed. Both Mg atoms are on general sites, but their site occupation factors are far from unity. Additionally the Mg−Mg-distances (Mg1−Mg1, 0.465 Å; Mg1−Mg2, 0.397/0.860 Å) are much too short for a simultaneous occupation. The free refinement of the site occupation factors yielded values of 0.2193(3) for Mg1 and 0.1482(15) for Mg2, which were in agreement with the expected minimum distances. In order to get a stable refinement, it was necessary to use isotropic and coupled displacement parameters. Finally *R*-values of $R_1(F) = 0.029$ and $wR_2(I) = 0.085$ were yielded for 1096 reflections and 87 free variables. Several single crystals were measured because of the problems with the Mg sites. It turned out that this is a general phenomenon in $Mg_{\sim 3}B_{50}C_8$. Diffuse scattering (streaks) and weak satellite reflections indicating a modulated structure and not a simple supercell were observed for all crystals investigated. This can be explained by the special situation of the Mg atoms (see Results and Discussion). For the (nearly) colorless crystals the sum of the Mg site occupation factors was always very close to the composition

(16) Vojteer, N.; Stauffer, J.; Hillebrecht, H.; Hofmann, K.; Panda, M.; Albert, B. *Z. Anorg. Allg. Chem.* **2009**, *635*, 653–659.
(17) Adasch, V.; Hess, K.-U.; Ludwig, T.; Vojteer, N.; Hillebrecht, H. *J. Solid State Chem.* **2006**, *179*, 2900–2907.
(18) Adasch, V.; Hess, K.-U.; Ludwig, T.; Vojteer, N.; Hillebrecht, H. *J. Solid State Chem.* **2006**, *179*, 2916–2926.
(19) Ludwig, T.; Hillebrecht, H. *J. Solid State Chem.* **2006**, *179*, 1622–1628.
(20) Adasch, V.; Hess, K.-U.; Ludwig, T.; Vojteer, N.; Hillebrecht, H. *J. Solid State Chem.* **2006**, *179*, 2150–2157.
(21) Adasch, V.; Hess, K.-U.; Ludwig, T.; Vojteer, N.; Hillebrecht, H. *Chem.—Eur. J.* **2007**, *13*, 3450–3458.
(22) Wörle, M.; Nesper, R. *J. Alloys Comp.* **1994**, *216*, 75–83.
(23) (a) Rogl, P. *Phase Diagrams of Ternary Metal−Boron−Carbon Systems*; ASM: Materials Park, OH, 1998. (b) Villars, P.; Calvert, D. *Pearson's Handbook, Crystallographic Data for Intermetallic Phases*; ASM International: Materials Park, OH, 1997.
(24) (a) Naslain, R.; Guette, A.; Hagenmüller, P. *J. Less-Common Met.* **1976**, *47*, 1. (b) Guette, A.; Barret, M.; Naslain, R.; Hagenmuller, P. *J. Less-Common Met.* **1981**, *82*, 325–334.
(25) Sheldrick, G. M. *SHELXL*; University of Göttingen: Göttingen, Germany, 1997.

Table 1. Crystallographic Data and Refinement for $Mg_3B_{50}C_8$

parameter	$Mg_3B_{50}C_8$
temperature	293(2) K
crystal shape	platelet
color	light-green
size	$0.2 \times 0.2 \times 0.04$ mm^3
crystal system	monoclinic
space group	$C2/m$ (No. 14)
unit cell	$a = 8.9384(13)$ Å
	$b = 5.6514(9)$ Å
	$c = 9.6021(13)$ Å
	$\beta = 105.86(1)°$
	$V = 466.58(8)$ Å^3
	$Z = 1$
d_{calcd}	2.525 g/cm^3
data collection	STOE IPDS II
Mo Kα	$\lambda = 0.710\,73$ Å (graphite monochromated)
	$0° \le \omega \le 180°$
	$\psi = 0°$; $\Delta\omega = 2°$
exposure time	300 s
θ range	$7° < 2\theta < 70°$
	$-14 < h < 13$
	$-9 < k < 9$
	$-16 < l < 15$
μ	0.20 mm^{-1}
absorption correction	none
R_{int}/R_σ	0.047/0.007
refinement	SHELXL;[25] full-matrix least-squares refinement on F^2
$N(hkl)$ measd, unique	3589, 1096
$N'(hkl)$ ($I > 2\sigma(I)$)	964
parameters refined	87
R-values	$R_1(F) = 0.0290$, $wR_2(F^2) = 0.0853$
all data	$R_1 = 0.0336$
weighting scheme[25]	0.0663/0.0168
extinction correction[25]	0.000(11)
goodness of fit	1.076
residual electron density (max, min, σ)	+0.50, − 0.28, 0.08 e$^-$/Å^3

Table 2. Atomic Coordinates, Equivalent Displacement Parameters (in Å^2), and Site Occupation Factors of $Mg_{\sim 3}B_{50}C_8$[a]

atom	site	x	y	z	sof	U_{eq}
Mg1	8*j*	0.7052(2)	0.3358(4)	0.5	0.2193(3)[b]	0.0052(2)[c]/U_{iso}
Mg2	8*j*	0.7683(3)	0.2202(5)	0.5	0.1481(15)[b]	0.0052(2)[c]/U_{iso}
C1	4*i*	0.13442(8)	0	0.94367(8)	1.000(4)	0.0045(2)
C2	4*i*	0.02208(9)	0	0.57526(9)	1.000(4)	0.0073(2)
B1	2*a*	0	0	0	0.997(3)	0.0066(2)
B2	4*i*	0.93410(9)	0.5	0.60812(8)	1.000(3)	0.0055(2)
B3	4*i*	0.12581(9)	0.5	0.60018(8)	1.000(4)	0.0057(2)
B4	4*i*	0.02093(9)	0.5	0.91679(8)	0.990(4)	0.0048(2)
B5	4*i*	0.22294(9)	0.5	0.91084(8)	1.000(4)	0.0048(2)
B6	8*j*	0.04885(6)	0.24148(11)	0.66446(6)	1.002(3)	0.0053(1)
B7	8*j*	0.10655(6)	0.75550(10)	0.85302(6)	1.003(3)	0.0049(1)
B8	8*j*	0.91773(6)	0.33789(10)	0.75755(6)	1.003(3)	0.0051(1)
B9	8*j*	0.74452(6)	0.83697(10)	0.75433(6)	0.990(4)	0.0051(1)

[a] esd values in parentheses. [b] Refined as free variable. [c] Coupled refinement, U_{iso}.

$Mg_3B_{50}C_8$. Details for the best refinement are listed in Table 1. Coordinates and thermal displacement parameters are given in Tables 2 and 3. Selected distances and angles are shown in Table 4.

Similar to other structure determinations of comparable compounds[15,17,18,20,21] the distinction between boron and carbon atoms is easy. With the correct labeling all thermal displacement parameters have nearly the same value. The ellipsoids show only small deviations from ideal spheres. The only exception is the C atom of the C_2 unit in $Mg_4B_{50}C_8$ and $Mg_3B_{50}C_8$. This is caused by the distribution of the Mg atoms. The very small absolute values of U_{eq} indicate a strong covalent bonding and are consistent with the high hardness of boron rich boride carbides.

Table 3. Anisotropic Displacement Parameters (in Å^2) of $Mg_{\sim 3}B_{50}C_8$[a]

atom	U_{11}	U_{22}	U_{33}	U_{12}	U_{13}	U_{23}
C1	0.0051(2)	0.0041(3)	0.0042(3)	0	0.0008(2)	0
C2	0.0124(3)	0.0044(3)	0.0045(3)	0	0.0011(2)	0
B1	0.0069(4)	0.0063(4)	0.0063(4)	0	0.0011(3)	0
B2	0.0058(3)	0.0065(3)	0.0045(3)	0	0.0017(2)	0
B3	0.0055(3)	0.0065(3)	0.0050(3)	0	0.0013(2)	0
B4	0.0052(3)	0.0051(3)	0.0043(3)	0	0.0014(2)	0
B5	0.0054(3)	0.0044(3)	0.0043(3)	0	0.0009(2)	0
B6	0.0066(2)	0.0046(2)	0.0045(2)	0.0000(2)	0.0011(2)	−0.0001(2)
B7	0.0056(2)	0.0045(2)	0.0042(2)	0.0002(2)	0.0009(2)	−0.0001(2)
B8	0.0049(2)	0.0055(2)	0.0049(2)	0.0000(2)	0.0014(2)	−0.0000(2)
B9	0.0053(2)	0.0055(2)	0.0044(2)	0.0004(2)	0.0010(2)	−0.0000(2)

[a] esd values in parentheses.

2.2. $Mg_4B_{50}C_8$. Black crystals of $Mg_4B_{50}C_8$ yielded a slightly larger unit cell of $a = 8.942(2)$ Å, $b = 5.6478(8)$ Å, $c = 9.614(2)$ Å, and $\beta = 105.60(3)°$. The measurement of 5033 intensities gave a data set of 983 independent reflections (868 with $I > 2\sigma(I)$). The refinement was started with the parameters of $Mg_3B_{50}C_8$. No significant differences were observed for B and C atoms including the very small and homogeneous displacement parameters, but the site occupation factor of the Mg atoms was higher. Again, several crystals were measured yielding similar results within small standard deviations. The resulting compositions were between $Mg_{\sim 3.5}B_{50}C_8$ and $Mg_{\sim 4.0}B_{50}C_8$. Again, diffuse scattering and weak satellite reflections were observed for all crystals. The best results were obtained for a crystal with a composition $Mg_4B_{50}C_8$, i.e., $sof_{Mg1} = 0.329(6)$ and $sof_{Mg2} = 0.183(6)$. The final R-values were $R_1(F) = 0.040$ and $wR_2(I) = 0.106$ with 983 reflections and 87 free variables.

2.3. $Mg_{2.4}B_{50}C_8$. The lattice parameters of the brown crystals were smaller ($a = 8.908(2)$ Å, $b = 5.6623(14)$ Å, $c = 9.605(3)$ Å, $\beta = 105.60(3)°$). The measurement of 4023 intensities gave a data set of 996 independent reflections (681 with $I > 2\sigma(I)$). The refinement with the known model showed only small differences for the B and C atoms, but the site of Mg2 was not occupied. The occupation factor for the remaining Mg atom increased to 0.299(3), and the composition was $Mg_{2.4}B_{50}C_8$. It is worth mentioning that the streaks and satellite reflections were no longer observed. The displacement parameters were uniform and very similar to those of $Mg_3B_{50}C_8$, so there is no sign of significant amounts of nitrogen. R-Values were $R_1(F) = 0.042$ and $wR_2(I) = 0.102$ with 996 reflections and 88 free variables.

Further details of the crystal structure investigations may be obtained from the Fachinformationszentrum Karlsruhe, D-76344 Eggenstein-Leopoldshafen (Germany) (fax, (+49)724-808-666; e-mail, crysdata@fiz-karlsruhe.de) on quoting the depository numbers CSD-419728 ($Mg_{2.4}B_{50}C_8$), CSD 419727 ($Mg_3B_{50}C_8$), and CSD-419729 ($Mg_4B_{50}C_8$).

3. Analyses/Characterization. Qualitative and quantitative analyses on selected single crystals were done by EDX and WDX measurements. Several single crystals of $Mg_{\sim 3}B_{50}C_8$ were checked by EDX (Jeol, JSM 6400 with Ge detector, sample fixed with conducting glue on a graphite platelet mounted on an aluminum sample holder). It was confirmed that magnesium is the only heavy element ($Z > 10$).

By WDX (Jeol, JXA 8200) a more detailed analysis especially in consideration of light elements ($4 < Z < 11$) was done to exclude their incorporation (oxygen, nitrogen) or to ensure its presence (carbon), respectively, because these problems frequently occur in boron rich borides. For the WDX measurement the single crystals used for the structure determinations by X-ray methods were fixed in a matrix with Ag/epoxy resin. They were polished to get a clear surface and to ensure the measurement of the interior of the crystal[10] and not of the surface which may be influenced by the contact to the melt or the single crystal isolation process. Boron, carbon, and magnesium were detected as the only elements with $Z > 4$. There were very small amounts of Cu (0.1%). The molar ratios B/C/Mg

Table 4. Selected Distances (in (Å) and Angles (in deg) in $Mg_{\sim 3}B_{50}C_8$[a,b]

Mg1−C2	2.167(2)[c]	Mg2−B3	2.182(2)	C1−B1	1.4460(7)		
Mg1−B3	2.205(1)	Mg2−B2	2.192(2)	C1−B5	1.6135(11)		
Mg1−B2	2.216(1)	Mg2−B3	2.198(2)	C1−B7	1.6159(7)[c]		
Mg1−B3	2.325(1)	Mg2−B2	2.207(2)				
Mg1−B2	2.333(1)	Mg2−B9	2.503(2)	C2−C2	1.3895(16)		
Mg1−B6	2.417(1)	Mg2−C2	2.512(3)[c]	C2−B6	1.5943(7)[c]		
Mg1−B6	2.424(1)	Mg2−B9	2.529(2)	C2−Mg1	2.169(2)[c]		
Mg1−B9	2.564(1)	Mg2−B8	2.536(2)	C2−Mg1′	2.170(2)[c]		
Mg1−B8	2.596(1)	Mg2−B8	2.563(2)				
Mg1−B9	2.601(1)	Mg2−B6	2.567(2)	B1−C1	1.4460(7)[c]		
Mg1−B8	2.636(1)	Mg2−B6	2.575(2)				
B2−B3	1.7179(12)	B3−B2	1.7179(12)	*B4−B4*	*1.7369(16)*	B5−C1	1.6135(11)
B2−B6	1.7921(8)[c]	B3−B6	1.7948(8)[c]	B4−B7	1.8174(8)[c]	B5−B7	1.7777(7)[c]
B2−B8	1.8234(9)[c]	B3−B9	1.8189(9)[c]	B4−B5	1.8224(11)	B5−B9	1.8174(9)[c]
B2−B3	*1.8653(11)*	*B3−B2*	1.8653(11)	*B4−B8*	1.8321(9)[c]	B5−B4	1.8224(11)
B6−C2	1.5943(7)	B7−C1	1.6135(7)	*B8−B9*	*1.7548(8)*	*B9−B8*	*1.7548(8)*
B6−B7	1.7414(9)	B7−B6	1.7414(9)	B8−B6	1.8174(8)	B9−B6	1.8089(8)
B6−B2	1.7921(8)	B7−B5	1.7777(7)	B8−B2	1.8234(9)	B9−B5	1.8174(9)
B6−B3	1.7948(8)	B7−B4	1.8174(8)	B8−B4	1.8321(9)	B9−B3	1.8189(9)
B6−B9	1.8089(8)	B7−B9	1.8255(8)	B8−B8	1.8323(12)	B9−B7	1.8255(8)
B6−B8	1.8174(8)	B7−B8	1.8400(8)	B8−B7	1.8400(8)	B9−B9	1.8425(12)

B1−C1−B3	102.52(8)	C2−C2−B2	121.14(3)[c]
B1−C1−B4	100.38(4)[c]	B2−C2−B2	117.72(7)
B3−C1−B4	115.82(3)[c]		
B4−C1−B4	117.54(6)	C1−B1−C1	180° (by symmetry)

[a] Exohedral B−B distances are in italics. Mg−Mg distances are omitted. [b] Refinement with disorder and partial occupation. [c] Occurs 2×.

were found to be 81.0:13.9:4.9. Calculated values for the composition of $Mg_3B_{50}C_8$ are 81.9:13.3:4.8.

The special properties of boron rich borides require a detailed quantitative analysis and special care on the refinement of single crystal data (for example, NaB_{15}/Na_2B_{29},[26] $NaB_5C/KB_5C/KB_6$[27]). In some previous contributions we have shown that the combination of high quality single crystal data and WDX/EDX measurements of single crystals yields reliable results for this special class of compounds ($Al_{2.7}B_{48}C_2$,[28] MgB_{17},[17] MgB_{12},[18] $MgB_{12}Si_2$,[19] $Mg_2B_{24}C$,[20] $MgB_{12}C_2$,[21] $Li_2B_{12}C_2$,[15] $LiB_{13}C_2$,[15] $Li_2B_{12}Si_2$[29]).

4. Microhardness. Microhardness was measured with a microhardness equipment MHT 10 (producer, A. Paar, Austria). A force of 2 N was generated within 10 s and applied for 15 s. The imprints of the indenters (Vickers hardness, square pyramid; Knoop, rhombic pyramid) were evaluated and converted into a value for the microhardness according to the usual procedures.[30]

5. IR and Raman Spectra. The FT-IR and FT-Raman measurements were performed with a Bruker IFS66v spectrometer. The IR sample was made of crystalline powder pressed with KBr to pellets. Raman measurements were carried out with a Nd:YAG laser with an output of 100 mW and 1000 scans on single crystals with a Raman microscope. Powder samples were prepared in 0.3 mm capillary and measured with an output of 400 mW and 5000 scans.

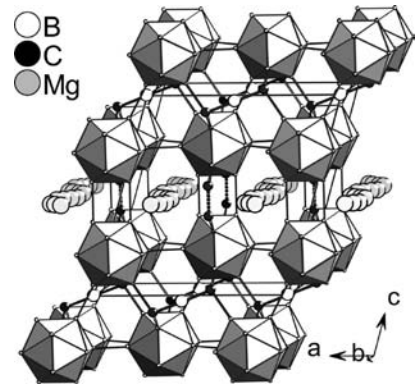

Figure 2. Crystal structure of $Mg_3B_{50}C_8$.

6. UV/Visible Spectra. The single-crystal-UV/vis spectra were measured in transmission at room temperature with a JASCO V-570 UV/vis/NIR photometer in a range from 200 to 2500 nm.

Results

According to the different conditions of synthesis, the Mg content shows a significant variation: $Mg_xB_{50}C_8$ with $x = 2.4-4$. $Mg_{\sim 3}B_{50}C_8$ (i.e., $x = 3$) is accessible as a main product, while $Mg_{\sim 2.4}B_{50}C_8$ and $Mg_{\sim 4}B_{50}C_8$ were only observed in small amounts as byproduct. Therefore, we focus the discussion on the phase with $x \approx 3$. Furthermore, it will be named as $Mg_3B_{50}C_8$ because the deviation from the integer number is very small.

$Mg_3B_{50}C_8$. The crystal structure of $Mg_3B_{50}C_8$ (Figure 2) is characterized by layers of B_{12} icosahedra. The icosahedra are quite regular (Figure 3). The endohedral B−B distances are spread over a range between 1.718 and 1.843 Å (∅ = 1.801 Å). Within the hexagonal layer each B_{12} icosahedron is coordinated by six icosahedra forming exohedral B−B bonds to four of them with a bond length of 1.755 Å. This explains the pseudohexagonal metric of the *ab* plane and its slight

(26) (a) Albert, B.; Schmitt, K. *Chem. Commun.* **1998**, 2373–2374. (b) Albert, B.; Hofmann, K.; Fild, C.; Eckert, H.; Schleifer, M.; Gruehn, R. *Chem.—Eur. J.* **2000**, *6*, 2531–2536. (c) Naslain, R.; Kasper, J. S. *J. Solid State Chem.* **1970**, *1*, 150–151.
(27) (a) Albert, B.; Schmitt, K. *Chem. Mater.* **1999**, *11*, 3406–3409. (b) Ammar, A.; Ménétrier, M.; Villesuzanne, A.; Matar, S.; Chevalier, B.; Etourneau, J.; Villeneuve, G.; Rodríguez-Carvajal, J.; Koo, H.-J.; Smirnov, A. I.; Whangbo, M.-H. *Inorg. Chem.* **2004**, *43*, 4974–4987.
(28) Meyer, D. Ph.D. Thesis, University Freiburg, Germany, 1999.
(29) Vojteer, N.; Schroeder, M.; Röhr, C.; Hillebrecht, H. *Chem. Eur. J.* **2008**, *14*, 7331–7342.
(30) DIN EN 6507.

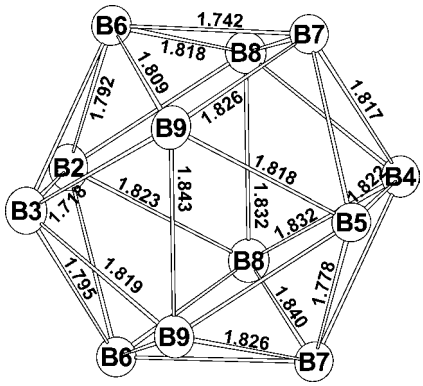

Figure 3. B_{12}-icosahedron in $Mg_3B_{50}C_8$. Ellipsoids are drawn with 95% probability and with mirror plane through B2/B3/B4/B5.

deviation from the ideal value ($c/a = 1.58 \neq \sqrt{3}$). This type of layer is a frequent motif in boron-rich borides and is also observed in *o*-$MgB_{12}C_2$,[21] $Mg_{1.13}B_{12}Si_2$,[31] SiB_3,[32] $Li_2B_{12}Si_2$,[29] $LiB_{13}C_2$,[15] and $Li_2B_{12}C_2$.[15] The layers are stacked in a sequence AABBCC parallel to the *ab* plane; i.e., two congruent layers form a double layer. The linkage between these double layers takes place via edges of the icosahedra. This type of connection is quite rare. Under the large number of boron-rich borides it is only observed in *m*-$MgB_{12}C_2$,[21] $Mg_{1.13}B_{12}Si_2$,[31] $Li_2B_{12}C_2$,[15] and $YB_{41}Si_{1.2}$.[33] The geometrical restrictions connecting icosahedra in that way may explain the long exohedral B−B bond of 1.864 Å (B2−B3). These are the longest B−B-distances in the structure, while the shortest ones (1.718 Å) are the distances B2−B3 within the icosahedron. The congruent double layers are connected by one exohedral bond (B4−B4: 1.734 Å) and stacked in a way as it is known from closest sphere packings.

The covalent network is completed by C_2 and linear CBC units. The C_2 units are between the congruent icosahedra. Each C atom is bonded to two icosahedra (Figure 4). The bonding angles B−C−C and B−C−C are quite close to 120°, so the short C−C distance of 1.389 Å can be explained as a double bond and a sp^2-like situation for carbon. A similar C_2 unit was already found in $Li_2B_{12}C_2$ (C−C, 1.374 Å), so $Mg_3B_{50}C_8$ represents the second example.

The CBC units link the double layers of congruent icosahedra. The central boron atom has two short distances to carbon (1.446 Å). According to the site symmetry, the C−B−C angle is 180°. The carbon atoms of the CBC unit are tetrahedrally coordinated by boron. One short bond occurs to the central B atom and three longer ones (1.613−1.616 Å) occur to three different icosahedra (Figure 4). The CB_4 tetrahedra are distorted with B−C−B angles between 100.4° and 117.5°. The B−C distances are comparable to those of other boron-rich boride carbides ($Mg_2B_{24}C$, 1.67 Å;[20] *o*-$MgB_{12}C_2$, 1.65−1.66 Å; *m*-$MgB_{12}C_2$, 1.64−1.67 Å[21]) but slightly longer than those of the C_2 unit (1.594 Å), which may be seen as a result from the different coordination (CN 4/CN 3) and bonding (sp^3/sp^2) because similar observations were made for $Li_2B_{12}C_2$ (B−C: 1.59 Å) and $LiB_{13}C_2$ (1.62 Å). Concerning the centers of the icosahedra, the CBC groups occupy octahedral voids. These (nearly) linear CBC groups are known from other boride carbides like Al_3BC_3,[9b] Sc_2BC_2,[34] Lu_3BC_3,[35] $Sc_3B_{0.75}C_3$,[36] $Ca_9Cl_8(CBC)_2$,[37] $Ca_5Cl_3C_2$-(CBC),[38] $La_9Br_6(CBC)_3$,[39] and $La_9Br_5(CBC)_3$.[40]

The two independent Mg atoms are placed in voids between the congruent layers. The distances to the surrounding B and C atoms (Mg−B, 2.18−2.64 Å; Mg−C, 2.17 Å) are comparable to those of other boride carbides of magnesium.[20,21] The surroundings (Figure 5) are built up by two faces and two edges of the B_{12} icosahedra and a C_2 unit. The resulting coordination number of 12 (i.e., 10 + 2) is plausible for boron rich borides. Both Mg sites are only partially occupied (Mg1, 0.2193(3); Mg2, 0.1482(15)). The site occupation factors sum up to 2.90(3); i.e., 3 of the 16 possible Mg positions are occupied. A detailed discussion is given below.

In total each B_{12} icosahedron has seven exohedral B−B-bonds (4 + 2 + 1) and five bonds to carbon. According to the structural features, the formula $Mg_3B_{50}C_8$ can be written as $Mg_3(B_{12})_4(CBC)_2(C_2)_2$. Because $Mg_3B_{50}C_8$ is nearly colorless and transparent, an electron-precise bonding situation is likely and the charge distribution follows well-known principles. According to Wade,[41] the icosahedra as closo-clusters with 12 exohedral 2e−2c bonds take up two electrons. Longuet-Higgins[42] showed this principle can be transferred from molecules to extended 3D structures with a covalent network of boron polyhedra. In $Mg_3B_{50}C_8$, Mg as an electropositive metal is a cation Mg^{2+} and supplies two electrons. The carbon atoms of the C_2 unit show four covalent bonds (one C−C double bond and two B−C single bonds), so they can be regarded as neutral. For the remaining CBC unit the charge +1 should be assumed with the positive charge mainly localized on the 2-fold bonded boron atom. A similar situation exists in $LiB_{13}C_2$ (or $LiB_{12}(CBC) = Li^+(B_{12}^{2-})(CBC^+)$), where the proposed charge distribution was confirmed by band structure calculations.[43] For other boron-rich borides like $Li_2B_{12}Si_2$[29] and *o*-$MgB_{12}C_2$[12] it was also shown that the formal charge of the cations is quite close to the idealized values. Therefore, the electronic situation is described by the formula $(Mg^{2+})_3(B_{12}^{2-})_4(CBC^+)_2(C_2)_2$, and $Mg_3B_{50}C_8$ is another example for the preference of electron-precise structures in boron-rich borides, boride carbides, and boride silicides of alkali and alkali earth metals.

Despite the structural similarity of the CBC units in $Mg_3B_{50}C_8$/$LiB_{13}C_2$ (B−C, 1.415 Å) and Al_3BC_3 (1.441 Å)/Sc_2BC_2 (1.475 Å)/Lu_3BC_3 (1.446 Å), the description is different. According

(31) Ludwig, T.; Hillebrecht, H. Presented at the 15th International Symposium on Boron, Borides and Related Materials, Hamburg, Germany, August 21−26, 2005; ISBB05. Publication in preparation.
(32) (a) Hirsche, B. Presented at the Symposium on Solid State Chemistry, Hirschegg, Austria, May/June 2002. (b) Salvador, J. R.; Blic, D.; Mahanti, S. D.; Kanatzidis, M. G. *Angew. Chem.* **2003**, *115*, 1973–1976; *Angew. Chem., Int. Ed.* **2003**, *42*, 1929–1931. (c) Hirsche, B. Ph.D. Thesis, University of Bayreuth, Germany, 2005.
(33) Higashi, I.; Tanaka, T.; Kobayashi, K.; Ishizawa, Y.; Takami, M. *J. Solid State Chem.* **1997**, *133*, 11.
(34) (a) Halet, J.-F.; Saillard, J.-Y.; Bauer, J. *J. Less-Common Met.* **1990**, *158*, 239–250. (b) Shi, Y.; Leithe-Jasper, A.; Tanaka, T. *J. Solid State Chem.* **1999**, *148*, 250–259.
(35) Oeckler, O.; Jardin, C.; Mattausch, H.; Simon, A.; Halet, J.-F.; Saillard, J.-Y.; Bauer, J. *Z. Anorg. Allg. Chem.* **2001**, *627*, 1389–1394.
(36) Shi, Y.; Bourgeois, L.; Leithe-Jasper, A.; Bando, Y.; Tanaka, T. *J. Alloys Compd.* **2000**, *298*, 99–106.
(37) Reckeweg, O.; DiSalvo, F.; Meyer, H.-J. *Z. Anorg. Allg. Chem.* **1998**, *625*, 1408–1410.
(38) Reckeweg, O.; Meyer, H.-J. *Angew. Chem.* **1998**, *110*, 3619–3621.
(39) Mattausch, H.; Simon, A. *Angew. Chem.* **1995**, *107*, 1764–1766; *Angew. Chem., Int. Ed. Engl.* **1995**, *34*, 1633–1635.
(40) Mattausch, H.; Simon, A.; Felser, C.; Dronskowski, R. *Angew. Chem.* **1996**, *108*, 1805–1807; *Angew. Chem., Int. Ed. Engl.* **1996**, *35*, 1685−1687.
(41) (a) Lipscomb, W. N. *Adv. Inorg. Chem. Radiochem.* **1950**, *1*, 117. (b) Wade, K. *Adv. Inorg. Chem. Radiochem.* **1976**, *18*, 1.
(42) Longuet-Higgins, H. C.; Roberts, M. d. V. *Proc. R. Soc., Ser. A* **1955**, *230*, 110.
(43) Balakrishnarajan, M. M.; Pancharatna, P. D.; Hoffmann, R. *New J. Chem.* **2007**, *31*, 473–485.

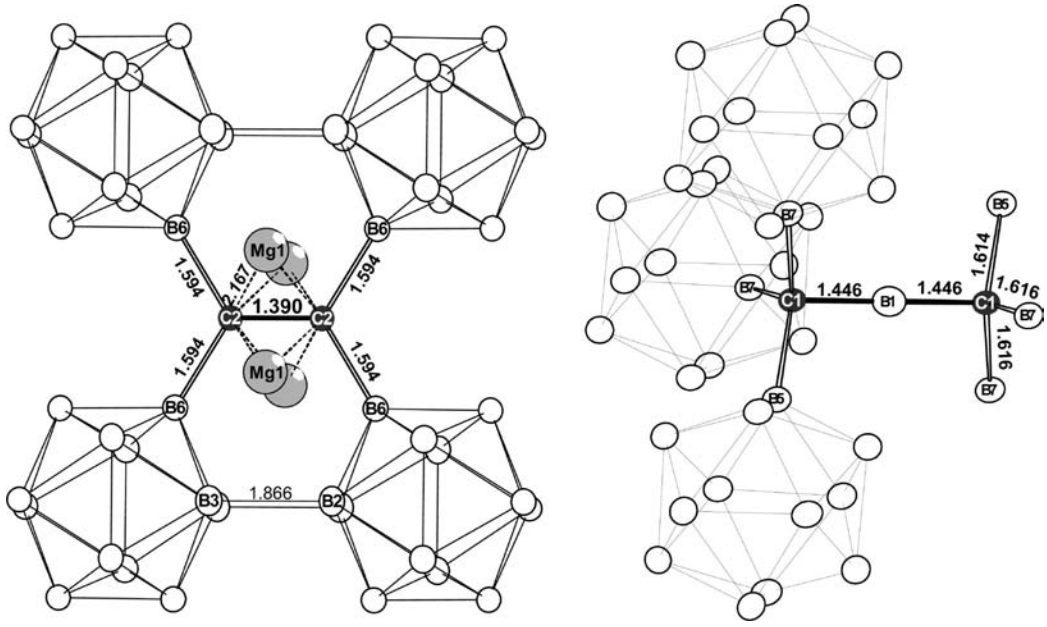

Figure 4. Surroundings of the C_2 unit (left) and the CBC unit (right) in $Mg_3B_{50}C_8$.

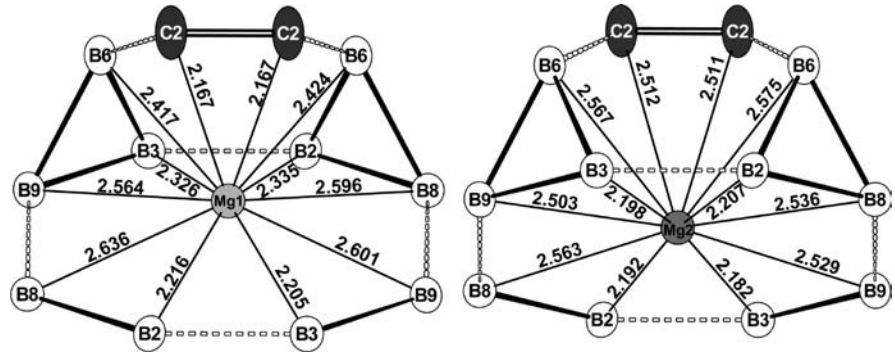

Figure 5. Surrounding of Mg in $Mg_3B_{50}C_8$.

to the (formally) positive charge of the B atom in the CBC unit, the distances are shortened and the force constants (frequencies in the vibrational spectra) enlarged with respect to a B−C single bond. Vice versa the (formally) double bond in Al_3BC_3 is reduced by the high negative charge of the CBC^{5-} unit. The effective bond order in the CBC unit of Al_3BC_3 is around 1.5 based on force constants (IR/Raman) and distances (Pauling's formula).[9b] In a previous publication[44] the band structure calculations reveal CBC^{5-} units with a significant covalent Al−C interaction.

$Mg_3B_{50}C_8$ continues the row of boron-rich boridecarbides of magnesium. It represents the most complex example for a crystal structure containing a covalent network of B_{12} icosahedra. Depending from the amount of additional carbon atoms or small building units (i.e., C_2, CBC) different types of frameworks are realized. In $Mg_2B_{24}C$ the B_{12} icosahedra form a tetragonal rod packing with isolated C atoms in tetrahedral and Mg^{2+} in octahedral voids between the rods. Each icosahedron has 10 exohedral B−B bonds to neighboring icosahedra and two bonds to carbon. In *m*-$MgB_{12}C_2$ the icosahodra show a cubic closest packing (*fcc*) with carbon atoms in all tetrahedral voids and Mg^{2+} in all octahedral voids. According to the higher content of carbon, each icosahedron shows eight exohedral B−B-bonds and four B−C bonds. In *o*-$MgB_{12}C_2$ the icosahedra have a hexagonal primitive arrangement. Mg^{2+} cations and C_2 units with an extremely long C−C distance of 1.73 Å and tetrahedrally coordinated C atoms are located in trigonal-prismatic voids. Here the icosahedron has six exohedral B−B bonds and six B−C bonds.

Remarkably $Mg_3B_{50}C_8$ combines the structural features of $Li_2B_{12}C_2$ and $LiB_{13}C_2$ in a 1 + 1 manner. In both Li compounds the B_{12} icosahedra form hexagonal layers connected by four exohedral bonds. These layers are connected by a linear CBC unit and one exohedral B−B bond ($LiB_{13}C_2$) or two exohedral bonds between the edge of the icosahedron and a C_2 unit with a C−C double bond ($Li_2B_{12}C_2$).

$Mg_{2.4}B_{50}C_8$ and $Mg_4B_{50}C_8$. The refinement of the single crystal data shows that the different colors of the crystals are connected to a variation of the Mg content. The black crystals have a higher Mg content. From the sum of the occupation factors of the two different Mg sites it results in a Mg content between $Mg_{3.5}B_{50}C_8$ and $Mg_{4.0}B_{50}C_8$. Similar to $Mg_3B_{50}C_8$ the refinement of Mg must be done with isotropic displacement parameters. For the distances within the covalent network of B_{12} icosahedra, C_2 and CBC groups are nearly unchanged, so they will not be discussed in detail.

(44) Jardin, C.; Hillebrecht, H.; Bauer, J.; Halet, J.-F.; Saillard, J.-Y.; Gautier, R. *J. Solid State Chem.* **2003**, *176*, 609–614.

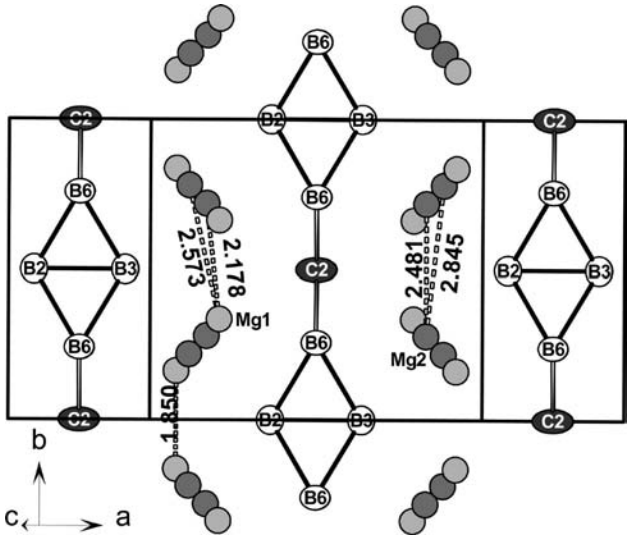

Figure 6. Structure of $Mg_3B_{50}C_8$ at $z \approx 0.5$.

In the brown crystals only one site is occupied and the Mg content is significantly lower ($Mg_{2.4}B_{50}C_8$). The refinement of the Mg atom with anisotropic displacement parameters was possible without peculiarities, and the anisotropy of the thermal displacement parameter of C2 vanished.

Mg Sites in $Mg_{2.4}B_{50}C_8$, $Mg_3B_{50}C_8$, and $Mg_4B_{50}C_8$. The problems with the localization of the Mg sites and the observation of diffuse diffraction and satellite reflections required a more detailed investigation. Figure 6 shows the structure of $Mg_3B_{50}C_8$ at $z \approx 1/2$. The 16 positions can be combined into four groups. The "outer" Mg atoms are Mg1, and the "inner" are Mg2. Within a group only one site can be occupied. The distances between the groups are as follows: Mg1−Mg1, 1.85 Å; Mg1−Mg2, 2.20/2.60 Å. An analysis shows that up to four positions can be occupied if unrealistically short Mg−Mg-distances (<2.3 Å) are excluded. Although this model is quite plausible, difference Fourier syntheses were done for all the three examples. Figure 7 shows the maps for $z \approx 1/2$. There are well-resolved maxima for $Mg_{2.4}B_{50}C_8$ with a distance of 0.9 Å. For $Mg_4B_{50}C_8$ and especially for $Mg_3B_{50}C_8$ the resolution is lower and the electron densities are higher. In all cases the maxima of the residual electron density correlate with the site occupation factors. In $Mg_{2.4}B_{50}C_8$ the maximum is 11.3 e^-/Å and 3.8 e^-/Å between them. The corresponding values in $Mg_3B_{50}C_8$ are 13.7 and 8.0 e^-/Å, and in $Mg_4B_{50}C_8$ they are 16.3 and 5.2 e^-/Å, respectively. The refinement ignoring the diffuse amounts simulates the distribution of the Mg atoms as a superposition of one ($Mg_{2.4}B_{50}C_8$) or two ($Mg_3B_{50}C_8$, $Mg_4B_{50}C_8$) Mg sites. The displacement parameters of the surrounding atoms show that only the position of the C_2 unit is significantly influenced by Mg. This is only observed for the samples with a higher Mg content. With lower Mg content there is enough space for the Mg atoms. Therefore, we conclude that the crystal structure is well-described by the refinement with a statistical occupation of the Mg sites and the highest possible Mg content results in the composition $Mg_4B_{50}C_8$.

Vibrational Spectra. Because many boron-rich borides are black, the measurement of IR and Raman spectra for this class of compounds is not very common. But $Mg_3B_{50}C_8$ is nearly colorless, so well-resolved vibrational spectra were obtained (Figure 8). They continue the row of other stoichiometric boron-rich borides ($Li_2B_{12}C_2$, $LiB_{13}C_2$,[15] $MgB_{12}Si_2$,[45] $Li_2B_{12}Si_2$[29]) and can be discussed by comparison. The structure of $Mg_3B_{50}C_8$ (or $Mg_3(B_{12})_4(C_2)_2(CBC)_2$) can be seen as a combination of $Li_2B_{12}C_2$ and $LiB_{13}C_2$ (= $LiB_{12}(CBC)$). For both Li compounds a detailed analysis of the vibrational spectra was possible including symmetry analysis, setup of spectra of expectation, and calculation of the frequencies on the basis of a force field.[45] It turned out that all modes are more or less coupled because of the strong interaction with the 3D covalent structure but the qualitative assignment of frequencies to building units is possible, especially for the region of the valence vibrations.

The Raman spectrum of $Mg_3B_{50}C_8$ shows a strong and sharp mode at 1436 cm^{-1} which can easily be attributed to the C−C-double bond ($Li_2B_{12}C_2$, 1477 cm^{-1}). The shoulders on both sides may be caused by the ordering of magnesium (see above). The signal at 1148 cm^{-1} probably corresponds to the B−C bonds ($Li_2B_{12}C_2$, 1194 cm^{-1}). Obviously there is no significant difference between the two different types of B−C bonds. The frequencies between 900 and 1050 cm^{-1} result from the internal modes of the B_{12} icosahedron, the exohedral B−B bonds, and contain the symmetric valence vibration of the CBC group (probably 1034 cm^{-1}). The latter occurs at 1156 cm^{-1} in $LiB_{13}C_2$; i.e., the shorter B−C distance of 1.413 Å corresponds to a higher frequency. In Al_3BC_3 the analogous values are 1044 cm^{-1} and 1.45 Å.[9a] For the assignment of the modes at lower wave numbers (deformation of B_{12} icosahedra, lattice modes, ...) more detailed investigations are necessary.

The IR spectrum shows very strong modes around 1090 cm^{-1}, which can certainly be assigned to the internal vibrations of B_{12} icosahedra and the exohedral B−B bonds because they are similarly observed in all boron-rich borides. The assignment of the signals at 1630 cm^{-1} to the antisymmetric valence mode of the CBC group is also quite clear ($LiB_{13}C_2$, 1628 cm^{-1};[15] Al_3BC_3, 1580 cm^{-1}).[9a] The shoulder at 1165 cm^{-1} may result from the exohedral B−C valence modes ($Li_2B_{12}C_2$, 1262 cm^{-1}; $LiB_{13}C_2$, 1263 cm^{-1}). Modes around 800 cm^{-1} and 500 cm^{-1} are similarly found in $Li_2B_{12}C_2$ (803 and 495 cm^{-1}1) and $LiB_{13}C_2$ (793 and 493 cm^{-1}). Although the spectrum below 900 cm^{-1} is well resolved, a detailed assignment requires again the extensive approach of force field based calculations. These investigations were successfully done for $Li_2B_{12}C_2$, $LiB_{13}C_2$,[45] and *o*-$MgB_{12}C_2$[12] and are in progress for $Mg_3B_{50}C_8$.

Optical Spectra. Figure 9 shows the UV−vis spectrum of a single crystal of $Mg_3B_{50}C_8$ measured in transmission. Between 420 and 500 nm the absorption changes significantly. The onset point in the low energy range can be determined to a value of 491 nm, which corresponds to an optical band gap of 2.7 eV. This value agrees very well with the crystal's color and is in a line with the optical properties and band gaps of other boron-rich borides. For colorless $B_{12}P_2$ we measured 400 nm (= 3.1 eV),[12] for the yellow crystals of $Li_2B_{12}Si_2$ and $MgB_{12}Si_2$ 545 nm (= 2.3 eV),[19,29] and for red MgB_7 630 nm (= 1.9 eV).[12] Unfortunately, a theoretical calculation of the band gap and other bonding properties is prevented for $Mg_3B_{50}C_8$ by the partial Mg occupation. Usually experimental and calculated values are in excellent agreement.[12,19,29]

Hardness Measurements. Values for hardness depend significantly on the conditions in which they were determined.[46] Therefore, we have measured the hardness of several well-

(45) Rotter, H. W.; Hillebrecht, H. Manuscript in preparation.
(46) Brazhkin, V.; Dubrovinskaia, N.; Nicol, M.; Novikov, N.; Rieder, R.; Solozhenko, V.; Zhao, Y. *Nat. Mater.* **2004**, *3*, 576–577.

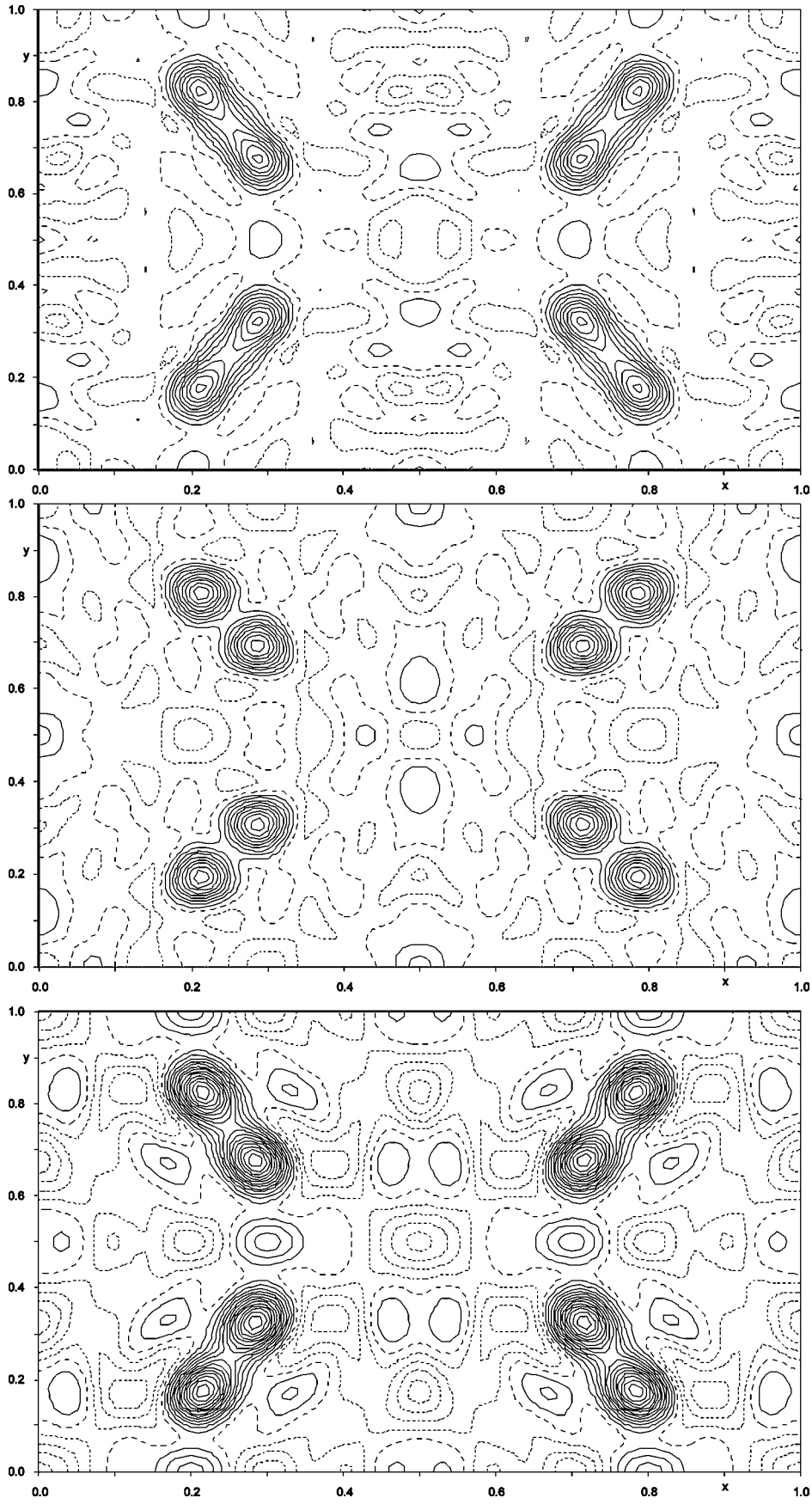

Figure 7. Difference Fourier maps at $z \approx 0.5$ for $Mg_3B_{50}C_8$ and $Mg_{\sim 4}B_{50}C_8$ (from top to bottom).

characterized hard materials (*c*-BN, B_4C, α-AlB_{12}) to get a reliable scaling. Furthermore, we have measured the microhardness of several boron-rich borides to get a feeling of how structural features influence the hardness.

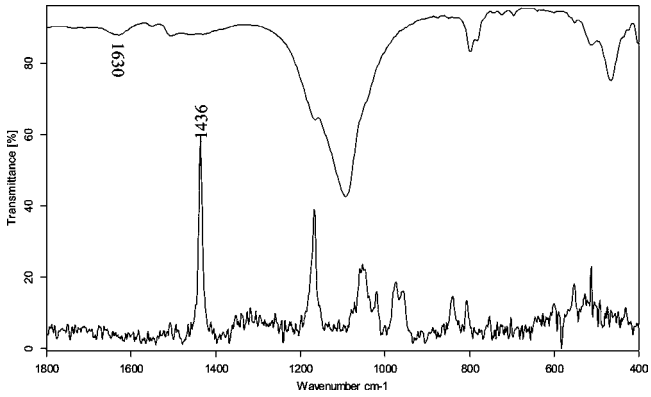

Figure 8. Vibrational spectra of $Mg_3B_{50}C_8$ (IR, top; Raman, bottom).

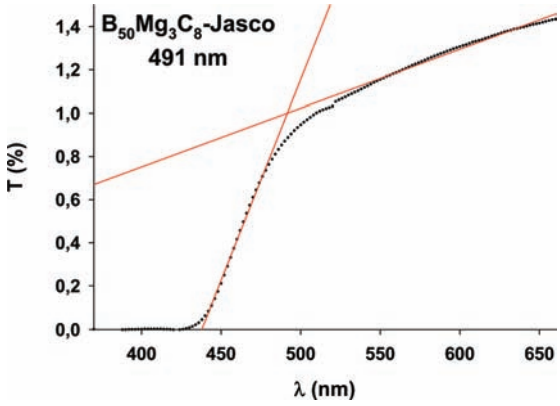

Figure 9. UV−vis spectrum in transmission of a $Mg_3B_{50}C_8$ single crystal.

For $Mg_3B_{50}C_8$, microhardness measurements according to Vickers H_V and Knoop H_K (see Experimental Section) revealed values of $H_V = 3286$ (32.0 GPa) and $H_K = 3165$ (31.5 GPa). The shapes of the imprints show the high brittleness of $Mg_3B_{50}C_8$ as expected for boron-rich borides (Figure 10). In particular, the Vickers method caused cracks. An overview of microhardness values measured with our setup is listed in Table 5. According to this, $Mg_3B_{50}C_8$ is the hardest boron-rich boride. An analysis of the dependence between microhardness and additional structural units shows that elements of the first row (B, C) favor higher hardness compared to second row elements (Si, P), in agreement with the higher bond strength. Compared to the other boron-rich boride carbides of Mg, the C_2 unit with double bond (and perhaps the CBC unit) seems to increase the microhardness.

Discussion

Molten metals are useful tools for synthesis and crystal growth of boron-rich borides. $Mg_3B_{50}C_8$ is another example of the versatility of this method. Furthermore, $Mg_3B_{50}C_8$ demonstrates the high flexibility of boron-rich borides to adopt a crystal structure, which can be described as a network with covalent bonds between boron polyhedra and additional "molecular" units. In sum, the resulting network is electron-precise according

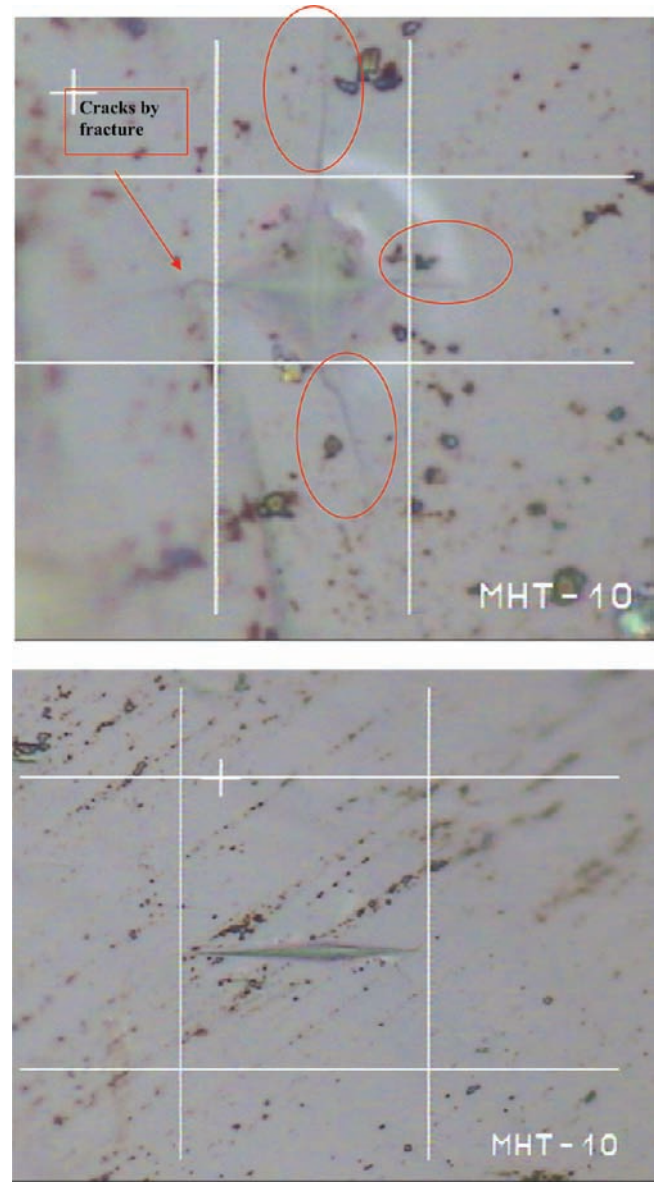

Figure 10. Microhardness measurements of $Mg_3B_{50}C_8$: imprints according to the methods of Vickers (top) with noticeable cracks and of Knoop (bottom).

to the simple rules of Wade and Longuet-Higgins. The validity of these rules was confirmed for several other boron-rich borides with similar crystal structures by state of the art band structure calculations.[12,29] Actually calculations for $Mg_3B_{50}C_8$ with respect to the partial Mg occupation are in progress.

Furthermore, $Mg_3B_{50}C_8$ is the first example of a boron-rich boride with a significant variation of the cation content. The deviations from the "ideal" composition, i.e., $Mg_3B_{50}C_8$, resulted in a significant change of the crystal's color. In general, physical properties can be varied in that way. Especially thermoelectric properties are of interest because boron-rich borides are a promising class of compounds for high temperature applications.[7,8] While n-type semiconducting phases are well-known (for example, B_4C[8]), p-type representatives are still missing. Here, the variation of the Mg content in $Mg_xB_{50}C_8$ may be of special importance.

The high stability of boron-rich borides whose structures based on an ionic separation in (formally) negative B_{12}^{2-} icosahedra linked by additional small fragments has recently

(47) Kotzott, D. Ph.D. Thesis, University Freiburg, Germany, 2009.
(48) Teter, D. M. *MRS Bull.* **1998**, *23*, 22–27.
(49) Adasch, V.; Hess, K.-U.; Hillebrecht, H. Ger. Offen. DE 102004014315 A1 20050512 CAN 142:413894 AN 2005:408030, 2005.
(50) Kotzott, D.; Hillebrecht, H. Unpublished results.
(51) Gurin, V.; Derkachenko, L. I. *Prog. Cryst. Growth Charact.* **1993**, *27*, 163–199.
(52) Prikhina, T. A.; Kisly, P. S. *AIP Conf. Proc.* **1991**, *231*, 590–593.

Table 5. Values for the Microhardness of Superhard Materials and Some Boron-Rich Borides Based on B_{12} Icosahedra

compd	H_V, GPa	H_K, GPa	structural units	ref	data from literature, GPa
c-BN	5108/50.0	4612/45.2	zinc blende	47	48−58[48]
$B_4C/B_{13}C_2$	3237/31.7	2787/27.3	CBC units	47	28−30[48]
$Mg_3B_{50}C_8$	3286/32.0	3165/31.5	C_2 (1.39 Å) and CBC units	this work	
m-$MgB_{12}C_2$		26	isolated C	21, 49	
o-$MgB_{12}C_2$	2482/24.0	2485/24.0	C_2 units (1.73 Å)	50	
MgB_7	2125/20.4	2005/19.3	B_2 units (2.26 Å)	47	
$MgB_{12}Si_2$	2075/19.9	1985/19.2	isolated Si	50	
$Li_2B_{12}Si_2$	2027/19.5	2075/20.0	isolated Si	29	
$B_{12}P_2$	2505/24.2	2134/20.9	P_2 units (2.24 Å)	47	
α-AlB_{12}	2345/22.8		B_{20} polyhedra	47	23[51]
$Al_3B_{48}C_2$	3152/31.0		isolated C	50	33.6[52]

shown up in the orthorhombic HP/HT polymorph of boron.[53,54] The structure consists of B_{12} icosahedra and additional B_2 units that link the icosahedra to a 3D framework. For this structure a more[53] or less[54] extended charge transfer is discussed. Independent from the description of the electronic situation, the hardness of orthorhombic boron (B_{28}) is higher and the compressibility lower than for α-rhombohedral boron.[53,54] According to Oganov et al.,[53] the reason for this is the ionicity of the structure. Another explanation might be the substitution of 2e−3c bonds between the icosahedra in α-rh boron by shorter bonds to the B_2 units, similar to the bonding situation in boron carbide $B_4C/B_{13}C_2$.

According to the findings for $Mg_3B_{50}C_8$, an alternative concept to obtain new (super)hard compounds is the substitution of exohedral 2e−2c bonds by bonds to small units with multiple bonds, for example, C_2 units with double bonds, CBC^+ units with short B−C distances, or new units containing nitrogen or oxygen. For the last we expect high hardness too because the covalent radii of N and O are smaller than for B and C. As we have learned from the structural chemistry of boron-rich borides, the high variability to form an electron-precise covalent network of B_{12} icosahedra and further small building units might result in new superhard materials.

Nevertheless it is not very likely that the hardness of boron-rich borides exceeds significantly a value of about 35 GPa because the hardness (i.e., bond strength) of the B_{12} icosahedra and the exohedral B−B bonds are a fundamental limit for this class of compounds. This may be extended for structures, where the exohedral B−B bonds are completely substituted by 2e−2c bonds to C, N, or O. According to Sung et al.[55] and Haines et al.,[56] short bond lengths (i.e., sum of covalent radii) and high ionicity (difference of electronegativity) increase the hardness, but until now no representatives are known.

The search for new (super)hard materials is still a challenge.[48,55−57] Despite strong efforts, diamond is still unbeaten. But the high "perfectness" of the diamond structure is a problem for changing its properties (i.e., band gap, conductivity, color, magnetic behavior, optical properties, ...). The same is true for diamond-related structures like *c*-BN, BC_2N,[58] or BC_5.[59] The usual synthetic access are HP/HT techniques according to the thermodynamic properties as high pressure phases. This is another drawback for a broader application and in some cases clear characterization of these interesting materials.

Recently great interest was caused by the high hardness of borides of 5d metals like ReB_2 and OsB_2.[60] Though the "real" values are still in discussion, the high hardness is obvious. It can be explained by the strong covalent B−B bonds and the strong metallic bonding between the high-melting 5d metals. Additionally the high number of shell electrons results in a low compressibility. But unfortunately the late 5d metals (i.e., Re, Os, Ir) are among the rarest elements on earth. So applications that demand them (for example, cutting tools) will be very expensive.

Conclusions

In conclusion boron-rich borides synthesized from metallic melts are very promising candidates for new hard and superhard materials with unique physical properties and a high potential for applications. In the case of $Mg_xB_{50}C_8$ ($x = 2.4-4$) more detailed investigations on the physical properties (conductivity, magnetism, optical and vibrational spectra, thermoelectricity) and band structure calculations are in progress. Especially NMR measurements are of interest. We expect distinct different signals for the two C atoms and a special situation for the linear coordinated B atom of the CBC group. EPR investigations can give insights into the influence of the Mg content on the bonding situation in $Mg_xB_{50}C_8$ ($x = 2.4-4$).

Acknowledgment. Thanks are due to the Bayerisches Geo-Institut (BGI, Universität Bayreuth, Germany) for the access to WDX measurements and to Detlev Krausse for his support.

Supporting Information Available: Complete list of authors for ref 54. This material is available free of charge via the Internet at http://pubs.acs.org. Additional data for the structure refinement are deposited at Fachinformationszentrum Karlsruhe.

JA102659D

(53) Oganov, A. R.; Chen, J.; Gatti, C.; Ma, Y.; Ma, Y.; Glass, C. W.; Liu, Z.; Yu, T.; Kurakevych, O. O.; Solozhenko, V. L. *Nature* **2009**, *457*, 863–867.
(54) Zarechnaya, E. Yu.; et al. *Phys. Rev. Lett.* **2009**, *102*, 185501. For complete list of authors, see Supporting Information.
(55) Sung, M.-C.; Sung, M. *Mater. Chem. Phys.* **1996**, *43*, 1–18.
(56) Haines, J.; Léger, J. M.; Bocquillon, G. *Annu. Rev. Mater. Res.* **2001**, *31*, 1–23.
(57) (a) Cohen, M. L. *Science* **1986**, *234*, 549. (b) Catlow, R. C. A.; Price, G. D. *Science* **1990**, *347*, 243.
(58) Solozhenko, V. I.; Andrault, D.; Fiquet, G.; Mezouard, M.; Rubie, D. C. *Appl. Phys. Lett.* **2001**, *70*, 1385–1387.
(59) Solozhenko, V. I.; Kurakevych, O. O.; LeGodec, Y.; Mezouar, M. *Phys. Rev. Lett.* **2009**, *102*, 015506.
(60) (a) Cumberland, R. W.; Weinberger, M. B.; Gilman, J. J.; Clark, S. M.; Tolbert, S. H.; Kaner, R. B. *J. Am. Chem. Soc.* **2005**, *127*, 7264–7265. (b) Kaner, R. B.; Gilman, J. J.; Tolbert, S. H. *Science* **2005**, *308*, 1268–1269. (c) Chung, H.-Y.; Weinberger, M. B.; Levine, J. B.; Kavner, A.; Yang, J.-M.; Tolbert, S. H.; Kaner, R. B. *Science* **2007**, *316*, 436–439. (d) Qin, J.; He, D.; Wang, J.; Fang, L.; Lei, L.; Li, Y.; Hu, J.; Kou, Z. *Adv. Mater.* **2008**, *20*, 4780–4783. (e) Chen, X.-Q.; Fu, C. L.; Krcmar, S.; Painter, G. S. *Phys. Rev. Lett.* **2008**, *100*, 19640. (f) Koehler, M. R.; Keppens, V.; Sales, B. C.; Jin, R.; Mandrus, D. *J. Phys. D: Appl. Phys.* **2009**, *42*, 095414. (g) Simunek, A. *Phys. Rev. B* **2009**, *80*, 060103.